

Large Earthquakes Recurrence Time in the Kefalonia Transform Fault Zone (KTFZ), Greece: Results from a physics-based simulator approach

Christos Kourouklas^{*,1}, Rodolfo Console^{2,3}, Eleftheria Papadimitriou¹, Vasileios Karakostas¹ and Maura Murru³

⁽¹⁾ Geophysics Department, School of Geology, Aristotle University of Thessaloniki, GR54124 Thessaloniki, Greece

⁽²⁾ Center of Integrated Geomorphology for the Mediterranean Area (CGIAM), Potenza, Italy

⁽³⁾ Istituto Nazionale di Geofisica e Vulcanologia (INGV), Rome, Italy

Article history: received January 13, 2023; accepted August 9, 2023

Abstract

Large earthquakes mean recurrence time (T_r) on specific fault segments is one of the primary input parameters for developing long-term Earthquake Rupture Forecast (ERF) models in a specific time span considering either a time-independent or an elastic rebound motivated renewal assumption. An attempt is made to define T_r on the major fault segments comprised in Kefalonia Transform Fault Zone (KTFZ), which is an active boundary demarcating from the west the area of central Ionian Islands, namely Lefkada and Kefalonia, and is associated with remarkably high seismic activity. Frequent large ($M_w \geq 6.0$) earthquakes are reported to have caused severe damage during the last six centuries. Although the number of large earthquakes (including both historical and instrumental) is satisfactory enough for regional hazard studies, their number become very limited when they are subdivided into subsets assigned to specific fault segments. Physics-based earthquake simulators are approaches to overcome recurrence intervals shortage, due to their ability to generate long lasting earthquake catalogs. The application of a physics-based simulator on the KTFZ, is attempted upon a detailed fault network model and implemented multiple times and with a wide range of input parameters, aiming at the definition of the most representative simulated catalog in respect to the observed regional seismicity. The most representative simulated catalog is finally used for investigating the recurrence behavior of large ($M_w \geq 6.0$) earthquakes and assessing whether the renewal model performs better than the Poisson model, after considering both individual and multiple ruptured segments scenarios.

Keywords: Physics-based earthquake simulator; Fault Interaction; Large Earthquakes Recurrence Time; Statistical Analysis; Kefalonia Transform Fault Zone, Greece

1. Introduction

Large earthquakes (e.g. $M \geq 6.0$) recurrence behavior on specific fault segments is one of the primary inputs for developing long-term Earthquake Rupture Forecast (ERF) models [Field, 2015]. Such models are capable to return the likelihood of the occurrence of near characteristic magnitude earthquakes [Schwartz and Coppersmith, 1984] in a specific time span and can be based on either a time-independent or an elastic rebound motivated renewal assumption. The key parameters of these models are the mean recurrence time, T_r , of large earthquakes and its aperiodicity, α [Convertito and Faenza, 2014]. In this respect, the identification of as many as possible large earthquakes (during both the historical and instrumental periods) being associated with distinctive fault segments is required for a precise and robust modelling of the recurrence time applications along with the selection of the appropriate statistical model. However, the observational recurrence intervals for each fault segment is often limited, ranging from 3 to 10 observations [Ellsworth *et al.*, 1999; Sykes and Menke, 2006] due to the long duration of the stress rebuilt and the shortage of earthquake catalogs. Additional data and methods such as palaeoseismic records [e.g. Biasi *et al.*, 2015], slip per event constraints [e.g. Ogata, 2002] and statistical methodologies such as Bayesian inference [Fitzenz, 2018] and the earthquake potential score (EPS) [Pasari *et al.*, 2023] are often used in order to refine the parameter space of recurrence models.

An alternative approach for supporting and improving the study of large earthquakes recurrence behavior is the development and application of physics-based simulator algorithms. These algorithms model the earthquake occurrence via numerical simulations using various approximations on well-known physical processes concerning the stress transfer and frictional properties of the fault segments along with kinematic and dynamic constraints [Tullis, 2012]. Starting from the first approaches of Rundle [1988], Robinson and Benites [1996] and Ward [2000], the concept of modeling the seismogenesis process through physics-based simulator algorithms became widely applied with several algorithms being proposed. Rundle *et al.* [2005] developed the Virtual California (VIRTCAL) earthquake simulator, which considered the geometric properties of the fault segments of the San Andreas Fault Zone to reproduce the seismicity associated with them according to the process of stress accumulation and release, also including a rupture weakening mechanism. This algorithm has undergone successive modifications and its current version has been renamed as Virtual Quake (VQ) [Schultz & Wilson, 2015; Schultz *et al.*, 2017]. Dieterich & Richards-Dinger [2010] and Richards-Dinger & Dieterich [2012] proposed the RSQSim simulator algorithm, which also relies on the stress accumulation and includes the effect of the Rate and State Constitutive Law [Dieterich, 1994] in the seismogenesis process. The ViscoSim earthquake simulator proposed by Pollitz & Schwartz [2008] and Pollitz [2011, 2012] is the only one that includes a viscoelastic model for the stress transfer and interaction between faults and stress transfer.

Following this concept, Console *et al.* [2015] proposed a stress driven simulator algorithm based on the modeling of the rupture growth, considering the long-term slip rate constraints on fault segments, that was firstly applied in the Corinth Gulf fault system in Greece. Over the years, the simulation algorithm has undergone significant evolutionary improvements, comprising new parameters for the identification of successive ruptures [Console *et al.*, 2017] and the inclusion of the afterslip process, modeled by a decaying Omori-like power law [Console *et al.*, 2018]. The latest version of the algorithm [Console *et al.*, 2020, 2022] incorporates the effect of the Rate and State Constitutive law proposed by Dieterich [1994] in the physical processes, leading to a stochastic manner of nucleation. The updated version of the simulator was successfully applied to model the seismicity of California [Parsons *et al.*, 2018], central Italy [Console *et al.*, 2020] and certain fault zones in Greece [Mangira *et al.*, 2020; Kourouklas *et al.*, 2021a,b; Console *et al.*, 2022].

In the current study, this lately updated version of the simulator algorithm is applied in the Kefalonia Transform Fault Zone (KTFZ). KTFZ runs along the western coastlines of the central Ionian Islands (Kefalonia and Lefkada), accommodating right-lateral strike slip motion and constituting the most active seismic zone in the broader Aegean area [Papazachos *et al.*, 1998]. It is characterized by frequent occurrence of large ($M_w \geq 6.0$) earthquakes during both the instrumental and the historical periods of seismicity [Papazachos and Papazachou, 2003]. Their temporal occurrence pattern can be explained by triggering due to the stress transfer among the adjacent fault segments [Papadimitriou, 2002]. This seismicity character provokes the detailed study of the recurrence times of large earthquakes, which could form the basis for the statistical analysis of these earthquakes' recurrence time behavior. The major fault segments of KTFZ are modelled, for the investigation of their large earthquakes mean recurrence time and their aperiodicity via the application and performance comparison of the Poisson model against the Brownian Passage Time (BPT) renewal model.

2. Seismotectonic Setting and Fault Network Definition of the KTFZ

The subduction of the oceanic lithosphere of Eastern Mediterranean under the continental Aegean microplate is the leading mechanism of the active deformation of the Aegean region [Papazachos and Comninakis, 1971]. It forms the Hellenic Arc (Figure 1), along with the extensional back Aegean arc region due to the roll back of the subducted plate [LePichon and Angelier, 1979]. The Kefalonia Transform Fault Zone (KTFZ; red rectangle in Figure 1) is recognized as the active boundary connecting the Hellenic subduction to the south and the continental collision of the Adriatic microplate and the Eurasia lithospheric plate to the north, with the collision front to run parallel both onshore and offshore along the western coastal areas of Greece and Albania [McKenzie, 1978; Clement *et al.*, 2000].

The KTFZ is characterized by right-lateral strike slip motion with a thrust component [Scordilis *et al.*, 1985; Kiratzi and Langston, 1991; Papadimitriou, 1993; Louvari *et al.*, 1999]. It is distinguished into two main branches, namely the Lefkada branch in its northern part, striking NNE-SSW and the Kefalonia branch to the south with a slightly different NE-SW strike. The mean thickness of the seismogenic layer along the KTFZ is equal to 12 km [Hatzfeld *et al.*, 1995]. The KTFZ exhibits the highest crustal deformation rates within the broader Aegean arc,

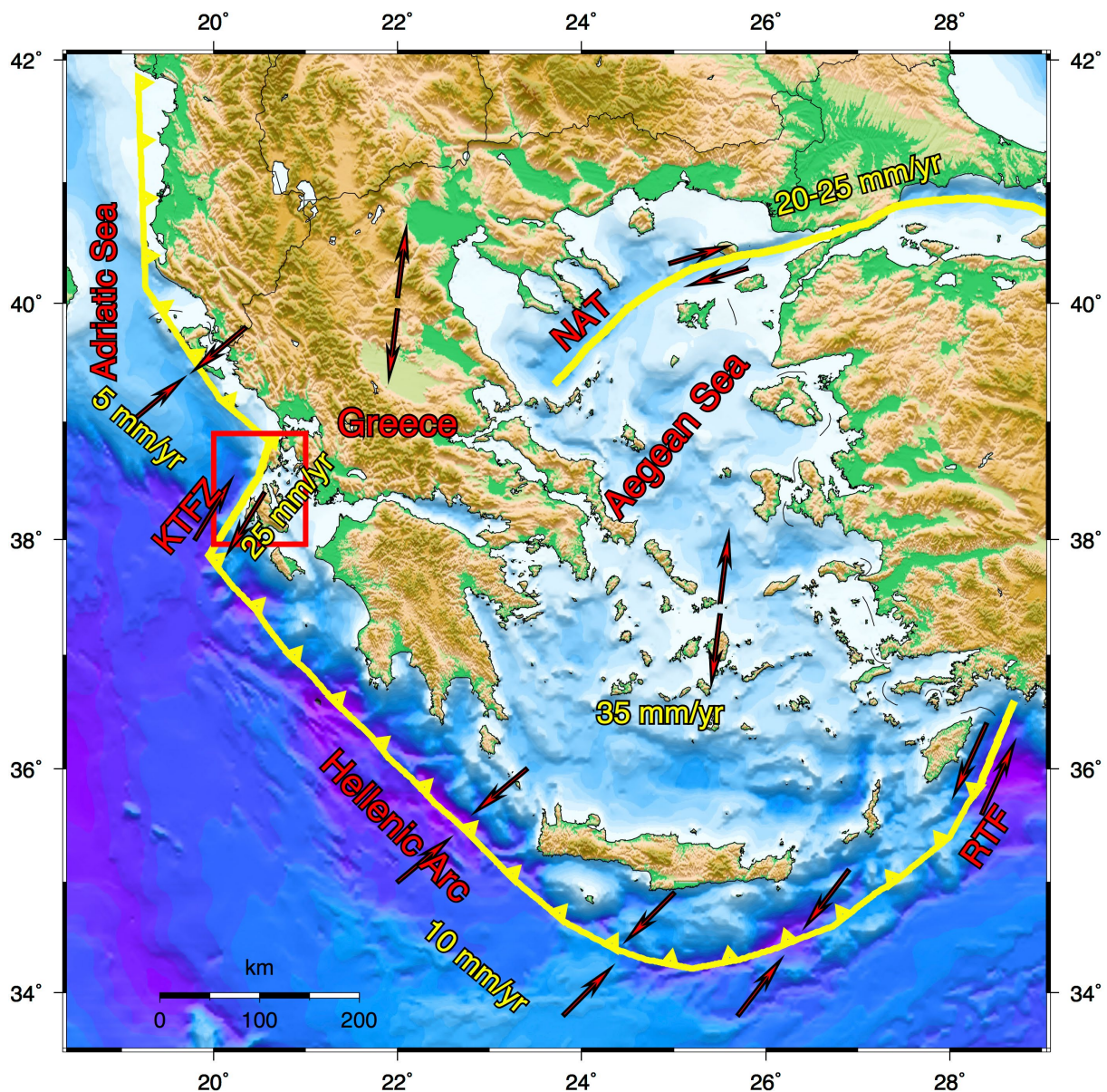


Figure 1. The active boundaries (solid yellow lines) and plate relative motions (red arrows) in the Aegean Sea area, along with their respective velocities [Papazachos *et al.*, 1998]. The Kefalonia Transform Fault Zone (KTFZ) is denoted with the red rectangle.

with rates presenting a gradual increase from north to south, taking values from 10 mm/yr for Lefkada Island up to 25 mm/yr for the southwestern margin of the Fault Zone [Kahle *et al.*, 1996; Cocard *et al.*, 1999]. Briole *et al.* [2015] suggested slip rates equal to 19.5 mm/yr along the Paliki Peninsula, in the western part of Kefalonia Island. More recently Briole *et al.* [2021] confirmed this gradual increase, proposing slip rates equal to 9.4 mm/yr in the northern part (Lefkada Island) and 14.3 mm/yr for the Paliki Peninsula. They also concluded that the KTFZ is the only region within the broader Aegean area where the tectonic deformation is fully coupled. This latter conclusion is in agreement with the results of Jenny *et al.* [2004], who compared the short- and long-term seismic moment rates with the long-term geodetic moment rates and showed that the total amount of the geodetic deformation is translated into seismic activity.

Frequent large earthquakes ($M_w \geq 6.0$) reported in both historical and instrumental catalogues. The $M_w \geq 6.0$ earthquakes that occurred since 2003 (Figure 2; 2003 with $M_w = 6.2$ in the northern part of Lefkada; 2014 with $M_w = 6.1$ and 6.0 in the Paliki Peninsula in Kefalonia; 2015 with magnitude $M_w = 6.5$ in the southern part of Lefkada), along with the one occurred offshore southeast of the Island of Kefalonia in 1983 with $M_w = 7.0$, attracts the research interest [Karakostas *et al.*, 2004; 2015, 2019; Ganas *et al.*, 2016; Papadimitriou *et al.*, 2017; Svigkas *et al.*, 2019; Kostoglou *et al.*, 2020; Bonatis *et al.*, 2021, among others] and thus a detailed segmentation model for KTFZ is available. The KTFZ is composed of five major dextral fault segments with strikes ranging from 11° to 40° , having lengths of 11–40 km and typical rake values for right-lateral strike slip faulting (Figure 2 and Table 1).

Starting from its northern part, along the western coasts of Lefkada Island, the Lefkada North and Lefkada South segments (S1 and S2 in Figure 2, respectively) are considered. The Lefkada North segment (S1), associated with the 2003 $M_w = 6.2$ earthquake, exhibits a NNE-SSW strike ($\varphi = 18^\circ$), dips east-southeast at an angle of 60° ($\delta = 60^\circ$), with a rake angle equal to -175° ($\lambda = -175^\circ$). Its dimensions equals to 16 and 10 km, for the length and the width,

Fault Segment		Strike [°]	Dip [°]	Rake [°]	L [km]	w [km]	Slip Rate [mm/yr]	Ref.
Name	Code							
Lefkada North	S1	18	60	-175	16	10	10	1,2
Lefkada South	S2	22	64	179	20	12	12	2, 3, 4
Kefalonia North	S3	12	57	157	12	10	19.5	5, 6
Kefalonia South	S4	12	57	157	12	10	19.5	5, 6
Offshore Kefalonia	S5	40	45	168	33	20	25	2, 7
Ainos	S6	300	35	100	35	24	4.9	8, 9, 10, 11
Step Over #1	S7	85	65	28	7	7	8	5
Step Over #2	S8	85	65	28	7	7	8	5
Step Over #3	S9	85	65	28	7	7	8	5

(1) Karakostas *et al.*, 2004; (2) Kahle *et al.*, 1995; (3) Briole *et al.*, 2021; (4) Papadimitriou *et al.*, 2017; (5) Karakostas *et al.*, 2015; (6) Briole *et al.* 2015; (7) Skordilis *et al.*, 1985; (8) Jenkins, 1972; (9) McKenzie, 1972; (10) Underhill, 1989; (11) D'Agostino *et al.*, 2020.

Table 1. Geometric and kinematic parameters of the fault network model for Kefalonia Transform Fault Zone. The thickness of the seismogenic layer is equal to 12 km for the entire the Fault Zone, with earthquake focal depths ranging between 3 and 15 km.

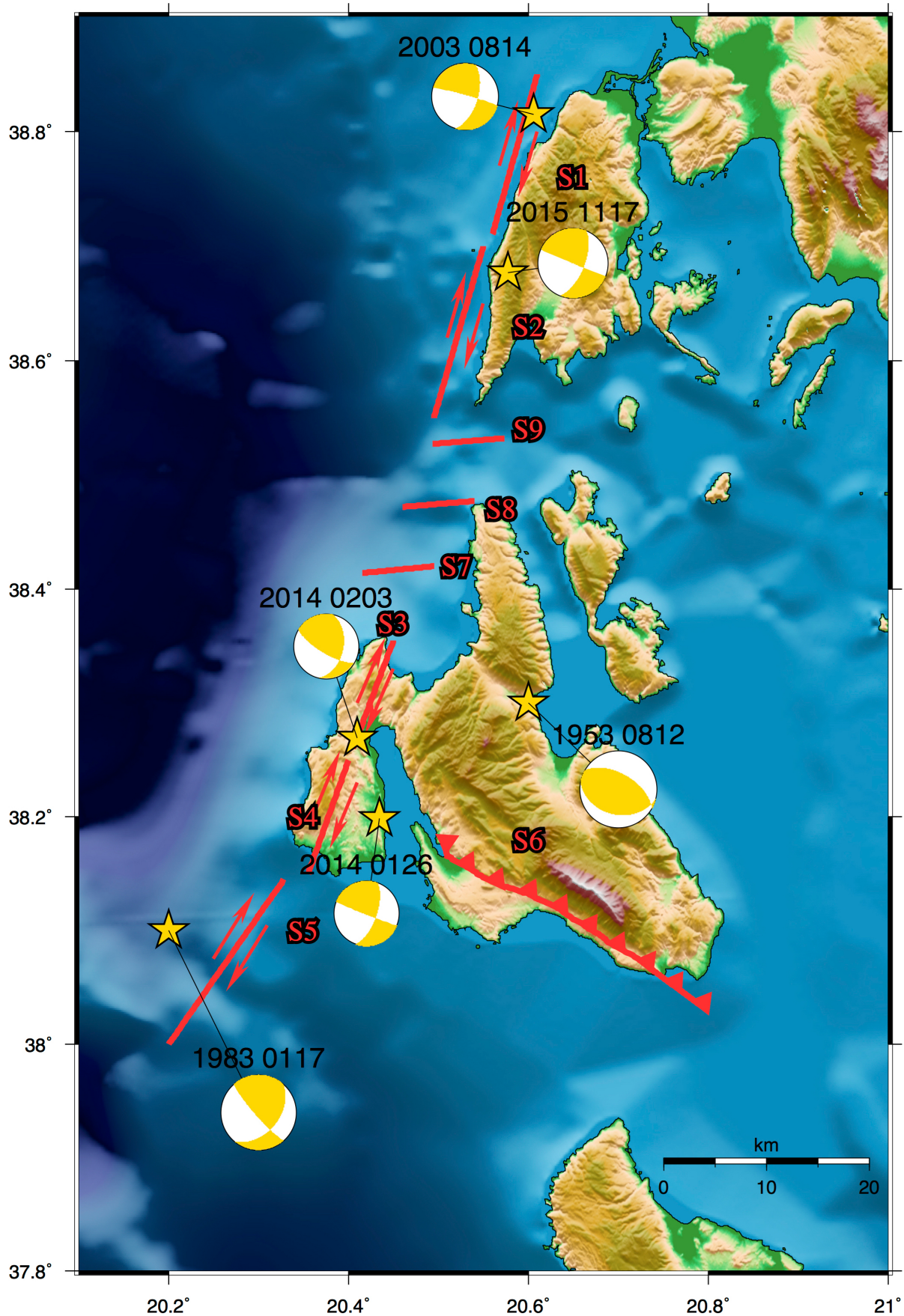


Figure 2. The recent (since 1953) large ($M_w \geq 6.0$) mainshocks occurred in Kefalonia Transform Fault Zone (yellow stars) along with their fault plane solutions [McKenzie, 1972; www.globalcmt.org]. Red solid lines depict the 6 major fault segments of Kefalonia Transform Fault Zone, along with the 3 secondary step over faults.

respectively [Karakostas *et al.*, 2004]. The Lefkada South segment (S2) is also striking NNE-SSW ($\varphi = 22^\circ$) and dips to the east-southeast with a slightly larger angle equal to 64° , and rake angle equal to 179° . The Lefkada South segment has a length equal to 20 km and a width equal to 12 km and is associated with the 2015 earthquake [Papadimitriou *et al.*, 2017]. Both fault segments are assigned with slip rates equal to 10 mm/yr (Table 1).

Moving to the south, in the western part of Kefalonia Island, the Kefalonia North and South fault segments (S3 and S4, respectively, in map of Figure 2) are extended. These two segments exhibit common geometric and kinematic characteristics and are associated with the 2014 Kefalonia doublet (the 26 January and the 3 February 2014 earthquakes with $M_w = 6.1$ and $M_w = 6.0$, respectively). Specifically, their dimensions are equal to $L = 12$ km and $w = 10$ km, having a strike equal to 12° and dip at an angle equal to 57° [Karakostas *et al.*, 2015]. The fifth and largest fault segment of KTFZ, namely the Kefalonia Offshore Fault Segment (S5) is associated with the $M_w = 7.0$ 1983 earthquake (Figure 2 and Table 1), has dimensions equal to $L = 33$ km and $w = 20$ km, NE-SW strike ($\varphi = 40^\circ$), dip angle equal to 45° ($\delta = 45^\circ$) and rake angle equal to 168° ($\lambda = 168^\circ$) [Scordilis *et al.*, 1985]. Karakostas *et al.* [2015] proposed the existence of a transition zone of secondary parallel rather extensional step-over fault segments, striking WSW-ENE and connecting the Lefkada with the Kefalonia branches (Figure 2 and Table 1). The southeastern part of Kefalonia Island is characterized by thrust faulting associated with the 1953 $M_w = 7.2$ large earthquake [McKenzie, 1972; Stiros *et al.*, 1994]. The causative fault of this large earthquake is the major thrust fault segment, namely the Ainos segment (S6 in map of Figure 2). Ainos fault segment strikes NW-SE ($\varphi = 300^\circ$), dips to NE and having rake angle 100° . Its length is equal to $L = 35$ km and its width is equal to $w = 24$ km [Jenkins, 1972; McKenzie, 1972; Underhill, 1989]. The Kefalonia North and South fault segments are assigned with slip rates equal to 19.5 mm/yr, whereas the offshore Kefalonia fault segment is getting the largest values of slip rate equal to 25 mm/yr. Each one of the step-over minor fault segments are assigned with a slip rate equal to 8 mm/yr, also used by Mangira *et al.* [2020]. Slip rate of the Ainos thrust fault segment is considered equal to 4.9 mm/yr, according to D'Agostino *et al.* [2020] (Table 1).

3. Physics-Based Simulator Outline

We present a brief outline of the updated version of the algorithm proposed and improved by Console *et al.* [2015, 2017, 2018, 2020, 2022]. The simulator algorithm is based on several physical constraints, such the geometric and kinematic parameters of a specific fault system. Each fault segment is represented as a quadrilateral plane source, onto which a normal grid of square cells is superimposed. The long-term slip rate is considered as uniformly distributed onto a certain fault segment which may vary from one segment to the other. Each cell is initially assigned with a stress value taken from a random distribution, which then increases with time due to the slow tectonic loading in terms of a backslip model.

The main improvement of the current version of the algorithm is that the nucleation process follows the Rate and State Constitutive Law [Dieterich, 1994], leading to a probabilistic manner of nucleation [Console *et al.*, 2020]. This is achieved by calculating the seismicity rate, R , in each cell with the equation:

$$R = \frac{r}{\left[\exp\left(-\frac{\Delta CFF}{A\sigma}\right) - 1 \right] \exp\left(-\frac{\Delta t}{\gamma_0 A\sigma}\right) + 1} \quad (1)$$

where r is the reference seismicity rate of each cell (defined as the seismicity rate R when $\Delta CFF = 0$), ΔCFF is the Coulomb Stress Change due to the coseismic slip of previous earthquakes, $A\sigma$ is the constitutive parameter expressing the response of the friction to a stress step change in a slip change [Toda and Stein, 2003], where A is a dimensionless fault constitutive parameter and σ the normal stress [Toda *et al.*, 1998], Δt is the time elapsed since the stress change on a given cell and γ_0 is the inverse of the reference tectonic stressing rate, $\dot{\tau}_r$ ($\gamma_0 = \frac{1}{\dot{\tau}_r}$). The reference seismicity rate adopted in the simulation, is obtained by dividing the slip rate of each fault segment in the model by the slip pertaining to an earthquake of average magnitude, assuming a Gutenberg-Richter magnitude distribution with $b = 1$, for earthquakes with magnitude exceeding the adopted threshold. Coulomb Stress Changes are computed by the equation:

$$\Delta CFF = \Delta\tau + \mu' \Delta\sigma_n \quad (2)$$

where $\Delta\tau$ is the shear stress change in the slip direction, $\Delta\sigma_n$ is the normal stress change, positive for extension normal to the observational fault plane, and μ' is the apparent coefficient of friction.

Setting an initial value of Δt in (1) the expected number N of earthquakes in this time interval is estimated for all cells from the occurrence rate. The probability of at least one earthquake occurring in the Δt is given by the Poisson distribution. If at least one cell exists where this probability exceeds a random number between 0 and 1, then the nucleation starts. If this is not the case, the probability is again computed for an increased value of Δt , and continues until a nucleation takes place.

Once the nucleation process starts, the strength of neighboring cells of a certain fault segment is reduced, resembling a weakening mechanism, and promoting the growth of the rupture. The length expansion of each rupture is limited by a given number of times the width of the fault segment, discouraging the rupture propagation in long distances. During the coseismic process, the stress decreases by a constant stress drop, Δp , in every cell that participates in the rupture, whereas in the surrounding cells the stress changes are calculated according to the ΔCFF (Eq. 2). A given cell can rupture more than once for the same earthquake. A rupture terminates when inside the activated area there are no more cells with stress exceeding their strength. Coulomb stress changes also contribute to the interactions among the causative and receiving segments, allowing the rupture expansion to neighboring fault segments, which are located within a distance limit (e.g. 5 km).

There are three key input parameters that must be specified at the start of the simulation. The first one is the product $A\sigma$ of the Rate and State law, affecting the nucleation process, the second one is the Strength Reduction Coefficient ($S-R$) associated with the fault weakening mechanism, governing the propagation of the rupture and the third one is the Aspect Ratio ($A-R$) parameter that controls the rupture propagation over long distances. The influence of the free parameters $S-R$ and $A-R$ was already analyzed by Console *et al.* [2015, 2017, 2018]. The Strength-Reduction coefficient ($S-R$) mainly controls the ratio between the number of small to large events. Small $S-R$ corresponds to simulated earthquake catalogs with fewer large earthquakes than the ones produced by using large parameter values. The effect of the Aspect-Ratio ($A-R$) value is mainly adjusts with the maximum magnitude of the simulated catalog but neither with the total number of events nor with the b -value of the simulated catalogs. Since the larger the $A-R$ value the larger the expansion of a rupture will be, the maximum magnitude of the catalog is also larger. Moreover, the main effect of $A\sigma$ in the simulation procedure is related with the occurrence rate of large earthquakes [Kourouklas *et al.*, 2021b].

4. Application of the simulator algorithm to the KTFZ

We applied the simulator algorithm considering each one of the six major fault segments of KTFZ as a rectangular planar source, consisting of 0.5×0.5 km square cells, and their kinematic and geometrical parameters shown in Table 1. Although the 3 minor step-over fault segment are not associated directly with large earthquakes, they are also included in the fault network model, aiming at an as representative as possible simulation of the seismicity within the KTFZ. The rigidity, μ , is taken equal to 3.3 GPa ($\mu = 3.3$ GPa), and the stress drop, $\Delta\sigma$, equal to 5.6 MPa ($\Delta\sigma = 5.6$ MPa) [Margaris and Hatzidimitriou, 2002].

We then assigned values to the free key parameters $A\sigma$, $S-R$ and $A-R$. A wide range of $A\sigma$ values are proposed in previous studies varying from 0.0012 to 0.6 MPa, as obtained from different earthquake sequences [Harris, 1998; Harris and Simpson, 1998]. Since the value of the product $A\sigma$ is not fixed, a range from 0.05 to 0.07 MPa with a step of 0.01 MPa was tested in the current study. The fault weakening mechanism is rather uncertain, because the relevant knowledge is based on indirect observations (e.g. past seismicity). Being a crucial factor of the simulator procedure, a range of $S-R$ values are also tested, starting from a value equal to 0.08, which represents strong faults, up to the value of 0.3, which implies enhanced weakening. The $A-R$ parameter is selected to be fixed and equal to 8 aiming to capture both the strike slip motion, which encourages large values of $A-R$, with the contribution of the thrust component in the final tectonic setting of KTFZ. Summarizing, the combination of the values of the three parameters was tested in the simulator application multiple times. Specifically, 12 different combinations stemmed from the aforementioned parameters values ranges, corresponding to 12 different simulated catalogs. The duration of each simulated catalog is set equal to 10 kyr with a warm-up period of 2 kyr, which were not taken into account in the final results.

Each triplet of input parameters yielded a simulated catalog with different total number of earthquakes, maximum magnitude, and b -values. The selection of the most representative simulated catalog is made after comparison

with observational data, taken from the catalog of Papazachos *et al.* [2010] and the regional catalog of Geophysics Department at the Aristotle University of Thessaloniki [1981, <http://geophysics.geo.auth.gr/ss>]. Specifically, each of the 12 simulated catalogs are compared with an integrated observational catalog that includes the earthquakes with $M_w \geq 4.0$ from 1980, $M_w \geq 4.5$ from 1970, $M_w \geq 5.0$ from 1950, $M_w \geq 5.5$ from 1911 and $M_w \geq 6.5$ from 1845, adopting the completeness thresholds suggested by Papazachos and Papazachou [2003].

The comparison is implemented by assessing the performance of each simulated catalog against the observational one via the application of the two sample Kolmogorov–Smirnov (KS2) [Stephens, 1974] and the Wilcoxon Rank-Sum (WR-S) [Wilcoxon, 1945; Mann and Whitney, 1947] tests, at a significance level of 0.05 ($\alpha = 0.05$). For this purpose, the cumulative earthquake number N_i of a certain simulated catalog for each magnitude bin is normalized by the corresponding period (N_i/period , in years) and then compared with the corresponding occurrence rates of the observational catalog, under the null hypothesis that the two rates come from the same population, against the alternative hypothesis that they come from different populations.

The statistic of the two sample Kolmogorov–Smirnov test is defined as:

$$D = \max(|F(x) - G(x)|). \quad (3)$$

where $F(x)$ and $G(x)$ are the empirical cumulative distribution functions (ecdf) of the two samples. The Wilcoxon Rank-Sum test compares two independent random variables F and G with sample sizes m and n , respectively, under the null hypothesis that the two samples come from the same distribution, similarly with the Mann-Whitney U-test. The Wilcoxon statistic, T , is calculated from the sum of the ranks according to:

$$T_F = \sum_{i=1}^m R_{F_i} \quad (4)$$

and

$$T_G = \sum_{j=1}^n R_{G_j} \quad (5)$$

The number of times that $F_i > G_j$ in an ordered arrangement, so called the Mann-Whitney statistic U is defined as:

$$U = \min(U_F, U_G) \quad (6)$$

where

$$U_F = mn + \frac{m(m+1)}{2} - T_F \quad (7)$$

and

$$U_G = mn + \frac{n(n+1)}{2} - T_G. \quad (8)$$

For both tests, the decision of rejecting or not the null hypothesis is based on the corresponding p -values, compared with the significance level. If p -value is greater than α ($p\text{-value} > \alpha$) then the null hypothesis can not be rejected. On the contrary, if p -value is lower than α ($p\text{-value} < \alpha$) the null hypothesis can be rejected.

Simulation	<i>p</i> -value	
	KS2	WR-S
#1 (0.05/0.08/8)	0.77	0.43
#2 (0.05/0.1/8)	0.91	0.44
#3 (0.05/0.2/8)	0.91	0.75
#4 (0.05/0.3/8)	0.66	1.00
#5 (0.06/0.08/8)	0.77	0.42
#6 (0.06/0.1/8)	0.92	0.57
#7 (0.06/0.2/8)	0.74	0.58
#8 (0.06/0.3/8)	0.66	1.00
#9 (0.07/0.08/8)	0.77	0.42
#10 (0.07/0.1/8)	0.92	0.53
#11 (0.07/0.2/8)	0.85	0.75
#12 (0.07/0.3/8)	0.66	0.98

Table 2. *p*-values of the two sample Kolmogorov-Smirnov (KS2) and Wilcoxon Rank-Sum (WR-S) tests at 0.05 level of significance ($\alpha = 0.05$) of the simulated versus observed annual occurrence rates.

Table 2 summarize the results of the applied tests for the comparison of the 12 simulated and the observational catalog. It is distinguished that in all the 12 cases the *p*-values of both tests values are quite larger than the significance level (0.05). Specifically, the *p*-values of the KS2 test range from 0.66 to 0.92, with 4 out of the 12 values being larger than 0.90 (*p*-value > 0.90), whereas the ones obtained from the WR-S test fluctuate between 0.42 and 1.0 (Table 2), showing a good performance with respect to the observational data. The case of the 6th simulation exhibits the best performance among the 12 simulated catalogs according to the KS2 test, since its *p*-value became the highest (*p*-value = 0.92). On the other hand, the *p*-value of the WR-S test is rather low (*p*-value = 0.57). Similarly, the 8th simulation exhibits the best performance according to the WR-S with *p*-value equal to 1 (*p*-value = 1.0), while the one of the KS2 test is again rather low (*p*-value = 0.66). The decision of the best performed simulated catalog is made considering a common *p*-value threshold for both tests, which is equal to 0.75. The case in which the *p*-values for both tests is larger than 0.75 is the one of the 3rd simulation, for which the *p*-values of KS2 and WR-S tests are equal to 0.91 and 0.75, respectively.

Figure 3 shows the summary of the annual occurrence rates of the 12 simulated catalogs (thin grey lines for the 11 out of 12 catalogs and thick blue line for the best performed one) in comparison to the occurrence rates of the observational catalog (thick red line). The comparison among rates of the observational versus the best performed catalogs reveals slight discrepancies in the magnitude bins from $M_w = 4.1$ to $M_w = 4.5$ but then adjusts with very good agreement up to the magnitude bin of $M_w = 6.8$. For magnitudes of $M_w = 6.9$ and above large discrepancies are again

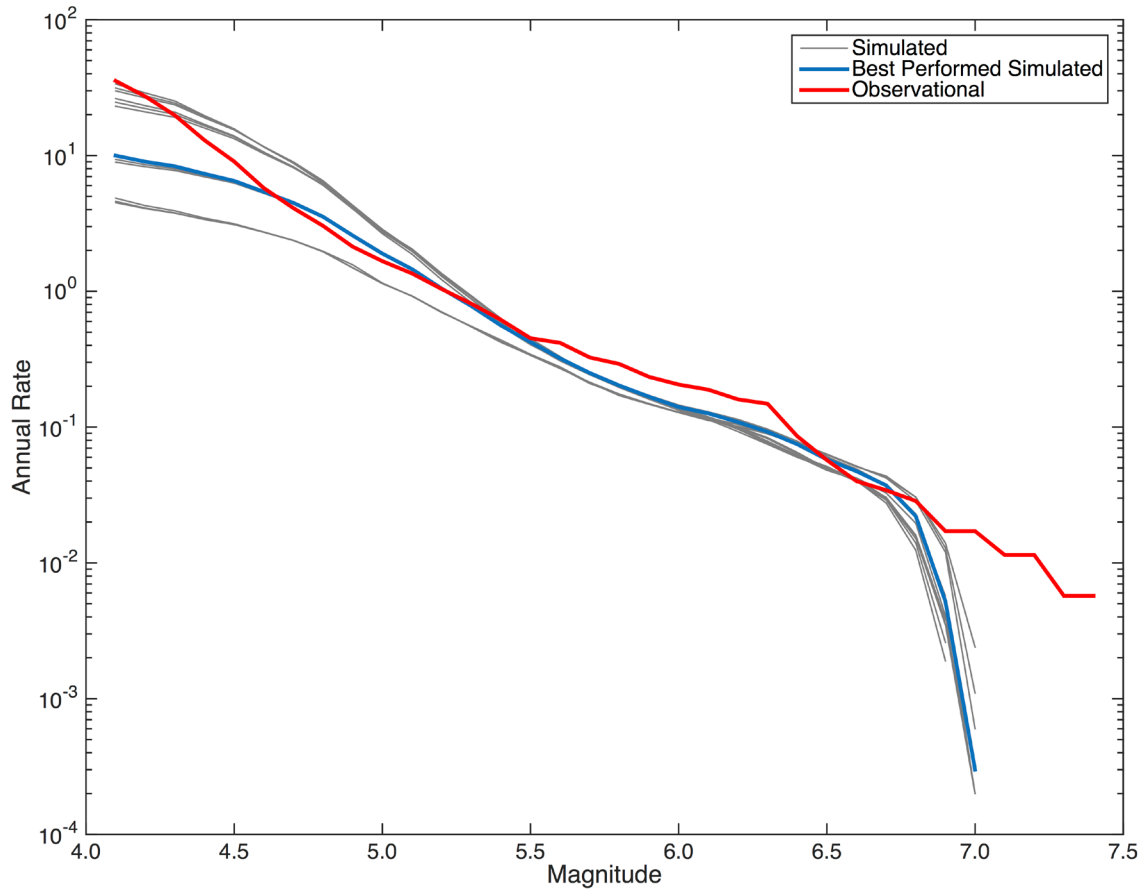


Figure 3. Summary of annual occurrence rates of the 12 simulated catalogs (thin grey lines), using different combination of the free input parameters ($A\sigma$, $S-R$, $A-R$). Annual occurrence rates of the best performed simulated catalog (Simulation 3; $A\sigma = 0.05$ MPa, $S-R = 0.2$, $A-R = 8$) is represented by the thick blue line, and the rates of the observational catalog with the thick red line.

observed, with the maximum reported simulated magnitude equal to $M_w = 7.0$, even though the maximum observed magnitude of the observational catalog is equal to $M_w = 7.4$, corresponding to a historical large earthquake, which is likely overestimated. The best performed simulated catalog ($A\sigma = 0.05$ MPa, $S-R = 0.20$, $A-R = 8$) is then used for the investigation of the large earthquakes recurrence pattern in KTFZ.

5. Large earthquakes ($M_w \geq 6.0$) Recurrence Models

For proceeding to the estimation of the large earthquakes mean recurrence time, T_r , a series of criteria are specified. Firstly, the minimum magnitude threshold above which the earthquakes may be considered as nearly characteristic, is set equal to 6.0 ($M_{thrI} \geq 6.0$). Such earthquakes are corresponding to a group of 330 ruptured cells. Since it is very likely that the resulting ruptures will be much larger than the sum of 330 cells, according to the geometrical properties of four out of six fault segments (Lefkada North and South, offshore Kefalonia and Ainos fault segments; Table 1), and the ability of the algorithm to allow the rupture propagation within adjacent fault segments, an additional magnitude threshold equal to 6.8 ($M_{thrII} \geq 6.8$) corresponding to at least 2065 ruptured cells, is also considered. Each earthquake above both magnitude thresholds is initially assigned to the segment where the nucleation starts. Additionally, the same earthquake is also assigned to more segments, if the corresponding rupture covers more than the 75% of the fault segment's area.

Considering the aforementioned rules, a detailed analysis of the ruptures resulted to $M_{thrI} \geq 6.0$ and $M_{thrII} \geq 6.8$ earthquakes was carried out. The simulator returns 1333 earthquakes with $M_{thrI} \geq 6.0$ in the best performed simulated catalog, from which the 219 are above M_{thrII} ($M_{thrII} \geq 6.8$), during the 10kyr. Table 3 summarizes the results of this analysis per fault segment. The Lefkada North and South fault segments participate in both single and multiple

ruptures resulting in earthquakes with magnitude up to $M_w = 6.6$. The three Kefalonia fault segments accommodate larger magnitude earthquakes, above the second higher magnitude threshold (with maximum magnitude equal to $M_w = 7.0$). Both results are consistent with the observations. The only case of single segment ruptures concerns the Ainos fault segment because it is isolated from the other ones and perhaps due to its different type of faulting.

Fault Segment	Single Segment Ruptures	Multiple Segment Ruptures	Ruptures above $M_{thrI} \geq 6.0$	Ruptures above $M_{thrII} \geq 6.8$	Maximum Simulated Magnitude
Lefkada North	74	92	166	—	6.6
Lefkada South	55	94	149	—	6.6
Kefalonia North	104	104	208	45	7.0
Kefalonia South	84	110	194	51	7.0
Offshore Kefalonia	363	97	460	95	7.0
Ainos	95	—	95	28	7.0

Table 3. Summary of single and multiple ruptures for the magnitude thresholds $M_{thrI} \geq 6.0$ and $M_{thrII} \geq 6.8$ for the five fault segments of KTFZ and Ainos thrust fault along with their maximum simulated magnitude values obtained from the best performing 10 kyr simulated catalogue.

Moving to the investigation of the, T_r , two different approaches are followed, aiming to assess whether the large earthquake occurrence in each fault segment is better described by the Poisson or by a renewal process. Poisson process can be expressed by the exponential distribution with probability density function (pdf) given by:

$$f(t|T_r) = \frac{1}{T_r} \exp \left\{ -\frac{t}{T_r} \right\} \quad (9)$$

where T_r is the mean recurrence time in each data sample. For modeling T_r as a renewal process the widely used Brownian Passage Time (BPT) distribution [e.g. Bantidi, 2022] proposed by Matthews *et al.* [2002] is applied. The pdf of the BPT model is given by:

$$f(t|T_r, \alpha) = \left(\frac{T_r}{2\pi\alpha^2 t^3} \right)^{\frac{1}{2}} \exp \left\{ -\frac{(t - T_r)^2}{2T_r\alpha t} \right\} \quad (10)$$

where T_r is the mean recurrence time and α is the aperiodicity, which can be considered as the analogous of the coefficient of variation of the normal distribution. It represents the level of the randomness taking values between 0 to 1 ($0 \leq \alpha \leq 1$) to address the physical meaning of the recurrence of large earthquakes. The parameters of both models are estimated through the Maximum Likelihood Estimation (MLE) method, along with their respective 95 per cent confidence intervals. The log-likelihood function of the Poisson process is defined by:

$$\ln L_p = (N - 1) \ln \left(\frac{1}{T_r} \right) - \frac{t_o(N)}{T_r} \quad (11)$$

where N is the number of observations and $t_0(N)$ is the occurrence time of the most remote event of the data sample, whereas the log-likelihood function of the BPT distribution is given by:

$$\ln L_{BPT} = \sum_{j=1}^{N-1} \ln \left\{ \frac{f(\Delta t(j))}{1 - F(t \leq \Delta t(j))} \right\} - \frac{t_0(N)}{T_r} \quad (12)$$

where $\Delta t(j)$ is the interevent time between the j th and the $j+1$ earthquakes and $f(\Delta t)$ and $F(t \leq \Delta t)$ are the pdf and the cumulative distribution function (cdf) of the BPT distribution, respectively. The performance of the applied models is examined in terms of their Akaike [Akaike, 1974] Information Criterion given by

$$AIC = -2\ln L + 2k \quad (13)$$

where $\ln L$ and k stands for the value of the log-likelihood function and the number of parameters of the assessed model, respectively.

Results of the MLE approach for both models and for the lower magnitude threshold ($M_{thrl} \geq 6.0$) are shown in Table 4 and Figure 4. The MLE method is implemented in the Lefkada North and South and in the Kefalonia North and South fault segments because their dimensions (Table 1) are compatible with this magnitude threshold as the characteristic one. It appears that the Kefalonia North and South Fault segments exhibit smaller mean recurrence times (equal to 48.24 and 51.53 years, respectively) than the Lefkada North and South segments (T_r equal to 60.14 and 67.26 years, respectively) due to their larger slip rate. The estimated aperiodicity, α , values of the Kefalonia North and South fault segments (equal to 0.63 and 0.66, respectively) are slightly larger than the ones of Lefkada segments, taking values equal to 0.48 and 0.51, respectively. The comparison of the applied models via the calculation of their respective AIC values reveals that in all the four cases the renewal model performs better than the Poisson model,

Fault Segment	$M_{thrl} \geq 6.0$					
	BPT	Exponential	$\log L_{BPT}$	$\log L_{Exp}$	AIC_{BPT}	AIC_{Exp}
Lefkada North	$T_r = 60.14$ yrs [55.74, 64.53] $\alpha = 0.48$ [0.42, 0.53]	$T_r = 60.14$ yrs [51.92, 70.48]	-769.28	-840.96	1532.56	1683.92
Lefkada South	$T_r = 67.26$ yrs [61.78, 72.75] $\alpha = 0.51$ [0.44, 0.57]	$T_r = 67.26$ yrs [57.62, 79.56]	-709.23	-770.8	1422.46	1543.76
Kefalonia North	$T_r = 48.24$ yrs [44.10, 52.38] $\alpha = 0.63$ [0.56, 0.70]	$T_r = 48.24$ yrs [42.29, 55.55]	-945.67	-1009.39	1895.34	2020.71
Kefalonia South	$T_r = 51.53$ yrs [46.72, 56.33] $\alpha = 0.66$ [0.59, 0.73]	$T_r = 51.53$ yrs [44.96, 759.65]	-903.88	-953.84	1811.76	1909.68

Table 4. MLE parameters estimates of the BPT (T_r and α) and exponential (T_r) distributions, along with their respective 95% confidence intervals and their respective AIC values for the Lefkada North and South and Kelalonia North and South fault segments for large earthquakes with $M_{thrl} \geq 6.0$.

Simulated Recurrence Times along KTFZ

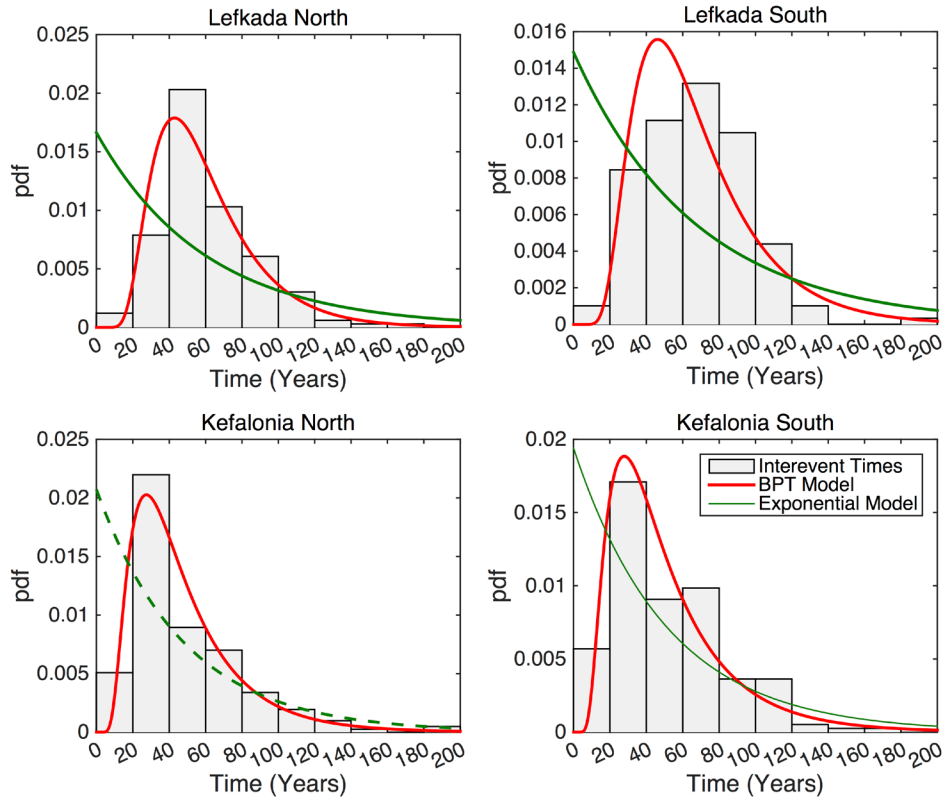


Figure 4. Probability density functions of Exponential (green lines) and BPT (red lines) distributions for the interevent times of large earthquakes with $M_{thrII} \geq 6.0$ for the Lefkada North, Lefkada South, Kefalonia North and Kefalonia South fault segments.

since its values are significantly smaller (Table 4). Figure 4 shows the probability density functions of both models along with the interevent times of simulated earthquakes with $M_{thrII} \geq 6.0$, which graphically evinces the better fit of the BPT distribution to the data in all cases.

The statistical analysis is then applied in recurrence intervals between successive earthquakes with $M_{thrII} \geq 6.8$ of Kefalonia North and South, offshore Kefalonia and Ainos fault segments, as reported in the best performed simulated catalog. It is worth to note that Kefalonia North and South fault segments participates only in multiple segment ruptures with $M_{thrII} \geq 6.8$, either rupturing together or playing a supportive role in ruptures nucleated on the offshore Kefalonia fault segment. The later segment is also participating in single segment ruptures with $M_{thrII} \geq 6.8$. As already stated, Ainos fault is the only one that ruptured individually in earthquakes with $M_{thrII} \geq 6.8$.

Focusing in the results of the statistical analysis for the higher magnitude threshold (Table 5), the estimated T_r values are fluctuating between 103 and 339 years. Offshore Kefalonia fault segment, assigned with the largest slip rate, exhibits the smallest mean recurrence time equal to $T_r = 102.92$ years. Additionally, its recurrence behavior is quasi-periodic according to the renewal model, since the estimated aperiodicity value is equal to $\alpha = 0.58$ (Table 5). The mean recurrence time, T_r , of the Kefalonia North and South fault segments is rather high equal to 216.75 and 180.56 years, respectively, indicating that these segments participate less frequently in multiple ruptures. Their aperiodicity values indicate a high aperiodic recurrence behavior, taking values equal to $\alpha = 0.73$ and $\alpha = 0.83$, respectively.

The largest mean recurrence time is observed in the simulated earthquake data of Ainos fault segment. Specifically, its estimated value is equal to $T_r = 338.95$ years, whereas its aperiodicity is equal to $\alpha = 0.35$ according to the BPT model. This aperiodicity value highlights the Ainos fault segment as the one with the most periodic recurrence behavior associated with $M_{thrII} \geq 6.8$ earthquakes. The corresponding values of the AIC (Table 5) again show that the renewal model performs better than the Poisson model, since in all cases the respective values are lower. This results could also be extracted from the visual comparisons among the respective probability density of the two applied distributions with respect to the interevent times data (Figure 5).

Fault Segment	$M_{thrII} \geq 6.8$					
	BPT	Exponential	$\log L_{BPT}$	$\log L_{Exp}$	AIC_{BPT}	AIC_{Exp}
Kefalonia North	$T_r = 216.75$ yrs [169.61, 263.88] $\alpha = 0.73$ [0.56, 0.91]	$T_r = 216.75$ yrs [164.65, 298.30]	-270.81	-280.66	545.62	563.32
Kefalonia South	$T_r = 180.56$ yrs [138.81, 222.31] $\alpha = 0.83$ [0.64, 1.00]	$T_r = 180.56$ yrs [139.37, 243.28]	-302.93	-309.80	609.86	621.60
Offshore Kefalonia	$T_r = 102.92$ yrs [90.83, 115.01] $\alpha = 0.58$ [0.49, 0.67]	$T_r = 102.92$ yrs [84.92, 127.36]	-496.09	-529.59	996.18	1062.18
Ainos	$T_r = 338.95$ yrs [294.26, 383.64] $\alpha = 0.35$ [0.25, 0.44]	$T_r = 338.95$ yrs [240.23, 514.34]	-526.31	-573.56	1056.62	1149.12

Table 5. MLE parameters estimates of the BPT (T_r and α) and exponential (T_r) distributions, along with their respective 95% confidence intervals and their respective AIC values for the Kefalonia North and South, offshore Kefalonia and Ainos fault segments for large earthquakes with $M_{thrII} \geq 6.8$.

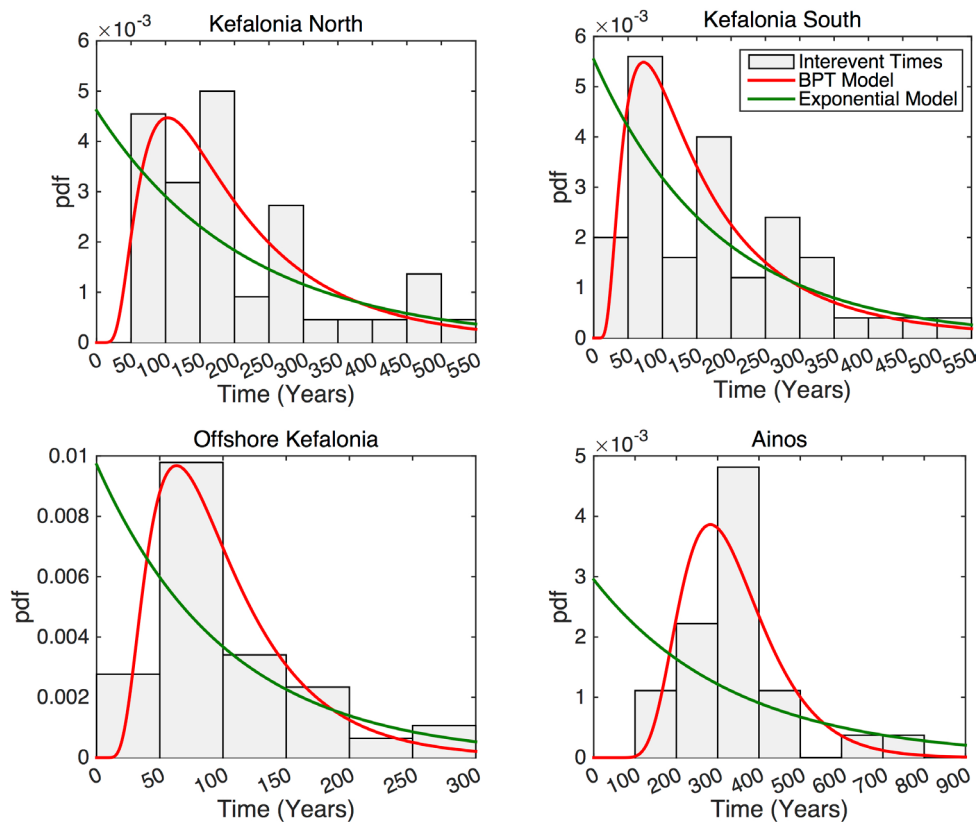


Figure 5. Probability density functions of Exponential (green lines) and BPT (red lines) distributions for the interevent times of large earthquakes with $M_{thrII} \geq 6.8$ for the Kefalonia North, Kefalonia South, offshore Kefalonia and Ainos fault segments.

6. Concluding Remarks

The successful application of the physics-based simulator algorithm in the fault segments of KTFZ has allowed the compilation of a simulated seismic catalogue lasting 10 kyr and containing 99862 earthquakes with $M \geq 4.1$, from which the 1333 are above the magnitude threshold of $M \geq 6.0$. The simulated catalogue achieves the replication of the observed seismicity, as the annual earthquake occurrence rates estimates are in good agreement with the observational data. The large number of the reported $M \geq 6.0$ earthquakes provides a sufficient number of earthquakes per certain fault segment, in order to study their recurrence behavior.

Emphasizing the large earthquakes occurrence, both single and multiple segmented ruptures are reported in the best performed simulated catalogue. A remarkable point arising from the results of the multiple ruptures is that the Kefalonia fault segments (Kefalonia North, Kefalonia South and offshore Kefalonia fault segments) are participating more frequently in multiple segment ruptures rather than the ones of Lefkada Island (Lefkada North and South). Their multiple segment ruptures are resulting in simulated earthquakes with magnitudes up to $M_w = 7.0$, whereas the maximum magnitude of Lefkada North and South segments reaches $M_w = 6.6$, in good agreement with the maximum observed magnitudes. The Ainos thrust fault segment in the eastern part of Kefalonia Island is the only one that ruptured individually, due to its large distance from the other fault segments and its considerable lower slip rate.

The estimated mean recurrence times, T_r , for the lower magnitude threshold, $M_{thrI} \geq 6.0$, exhibits slight differentiation between the Lefkada (North and South) and Kefalonia (North and South) fault segments. Specifically, T_r is taking values of about 60-70 years for the Lefkada North and South segments, and it is equal to almost 50 years for the Kefalonia North and South ones. When the magnitude threshold of $M_{thrII} \geq 6.8$ is considered the differentiations of T_r are becoming more significant among segments. More specifically, T_r is ranging between 102.92 and 338.95 years for the four segments (Kefalonia North and South, offshore Kefalonia and Ainos), when the $M_{thrII} \geq 6.8$ is set. The comparison between the memoryless Poisson and the BPT models by applying the Akaike Information Criterion reveals that in all cases and for both magnitude thresholds the renewal performs better than the Poisson model. This result supports the elastic rebound motivated behavior [Reid, 1911] of the large earthquakes occurrence in KTFZ.

Following the results of model comparison, the estimated aperiodicity, α , values of the BPT distribution indicate that the occurrence of large earthquakes with $M_{thrI} \geq 6.0$ is characterized by quasi-periodic behavior. Specifically, the Lefkada North and South segments are resulting in aperiodicity values equal to $\alpha = 0.48$ and $\alpha = 0.51$, respectively, whereas the Lefkada North and South faults are taking values equal to $\alpha = 0.63$ and $\alpha = 0.66$, respectively. Recurrence behavior of earthquakes with $M_{thrII} \geq 6.8$ exhibit larger variations from one segment to another. Ainos fault segment is the one with the most periodic behavior ($\alpha = 0.35$), possibly due to the fact that it is isolated from the other ones and does not interact with them. For the other three segments in Kefalonia Island, namely the offshore Kefalonia, Kefalonia North and Kefalonia South, the aperiodicity indicates variation from quasi-periodic behavior for the offshore Kefalonia segment to highly aperiodic for Kefalonia North and Kefalonia South fault segments.

These results offer valuable insights into the occurrence of large earthquakes along KTFZ and hold significant potential when combined with additional observational data. They can contribute to the development of robust models for forecasting large earthquake occurrences and generating Earthquake Rupture Forecasts over a specific time span. These forecasts can be based on both single and multiple rupture scenarios for the fault zone.

Acknowledgements. The constructive comments of two anonymous reviewers are greatly appreciated and contributed to the significant improvement of the manuscript. The historical and instrumental earthquake catalogues of Geophysics Department of the Aristotle University of Thessaloniki (<http://geophysics.geo.auth.gr/ss>). Maps and graphs are generated using the GMT software [Wessel *et al.*, 2013] and MATLAB software (<http://www.mathworks.com/products/matlab>). Fault plane solutions data used in this paper came from <https://www.globalcmt.org/> and other resources listed in the References Section. The study is partially financially supported by artEmis Project funded by the European Union, under Grant Agreement nr 101061712. Views and opinions expressed are however those of the author(s) only and do not necessarily reflect those of the European Union or European Commission-Euratom. Neither the European Union nor the granting authority can be held responsible for them. Geophysics Department Contribution 967.

References

- Akaike, H. (1974). A new look at the statistical model identification, *IEEE Trans. Autom. Control*, AC-19, 716-723, doi:10.1109/tac.1974.1100705.
- Aristotle University of Thessaloniki, 1981. Aristotle University of Thessaloniki seismological network. *Inter. Fed. Dig. Seis. Net*, doi:10.7914/SN/HT.
- Bantidi, T.M. (2022). Inter-occurrence time statistics of successive large earthquakes: analyses of the global CMT dataset, *Acta Geophys.*, 70, 2603-2619.
- Briole, P., P. Elias, I. Parcharidis, C. Bignami, G. Benekos, S. Samsonov, C. Kyriakopoulos, S. Stramondo, N. Chamot-Rooke, M.L. Drakatos and G. Drakatos (2015). The seismic sequence of January-February 2014 at Cephalonia Island (Greece): constraints from SAR interferometry and GPS, *Geophys. J. Int.*, 203, 1528-1540, doi: 10.1093/gji/ggv353.
- Briole, P., A. Ganas, P. Elias and D. Dimitrov (2021). The GPS velocity field of the Aegean. New observations, contribution of the earthquakes, crustal blocks model, *Geophys. J. Int.*, 226, 468-492, doi: 10.1093/gji/ggab089.
- Bonatis, P., A. Akinci, V. Karakostas, E. Papadimitriou and G. Kaviris (2021). Near-Fault Broadband Ground Motion Simulation Applications at the Central Ionian Islands, Greece, *Pure Appl. Geophys.*, 178, 3505-3527, doi:10.1007/s00024-021-02825-9.
- Clement, C., A. Hirn, P. Charvis, M. Sachpazi and F. Marnelis (2000). Seismic structure and the active Hellenic subduction in the Ionian Islands, *Tectonophysics*, 329, 141-156.
- Cocard, M., H.G. Kahle, Y. Peter, A. Geiger, G. Veis, S. Felekis, D. Paradissis and H. Billiris, (1999). New constraints on the rapid crustal motion of the Aegean region: recent results inferred from GPS measurements (1993-1998) across the West Hellenic Arc, Greece, *Earth Planet. Sci. Lett.*, 172, 1-2, 39-47.
- Console, R., R. Carluccio, E. Papadimitriou and V. Karakostas (2015). Synthetic earthquake catalogs simulating seismic activity in the Corinth Gulf, Greece, fault system, *J. Geophys. Res.*, 120, 326-343, doi:10.1002/2014JB011765.
- Console, R., A. Nardi, R. Carluccio, M. Murru, G. Falcone and T. Parsons (2017). A physics-based earthquake simulator and its application to seismic hazard assessment in Calabria (Southern Italy) region, *Acta Geophys.*, 65, 243-257, doi:10.1007/s11600-017-0020-2.
- Console, R., P. Vannoli and R. Carluccio (2018). The seismicity of Central Apennines (Italy) studied by means of a physics-based earthquake simulator, *Geophys. J. Int.*, 212, 916-929, doi:10.1093/gji/ggx451.
- Console, R., M. Murru, P. Vannoli, R. Carluccio, M. Taroni and G. Falcone (2020). Physics-based Simulation of Sequences with Multiple Mainshocks in Central Italy, *Geophys. J. Int.*, 223, 526-542, doi:10.1093/gji/ggaa300.
- Console, R., R. Carluccio, M. Murru, E. Papadimitriou and V. Karakostas (2022). Physics-Based Simulation of Spatiotemporal Patterns of Earthquakes in the Corinth Gulf, Greece, Fault System, *Bull. Seismol. Soc. Am.*, 112, 98-117, doi:10.1785/0120210038.
- Convertito, V. and L. Faenza (2014). Earthquake Recurrence. In: Beer, M., Kouglioumtzoglou, I. A., Patelli, E., Siu-Kui Au, I. (eds) *Encyclopedia of earthquake engineering*. Springer, Berlin, 1-22, <https://doi.org/10.1007/978-3-642-36197-5-236-1>.
- D'Agostino, N., M. Metois, R. Koci, L. Duni, N. Kuka, A. Ganas, I. Georgiev, F. Jouanne, N. Kaludjerovic and R. Kandic (2020). Active crustal deformation and rotations in the southwestern Balkans from continuous GPS measurements, *Earth Planet. Sci. Lett.*, 539, 116246, doi: 10.1016/j.epsl.2020.116246.
- Dieterich, J. (1994). A constitutive law for rate of earthquake production and its application to earthquake clustering, *J. Geophys. Res.*, 99, 2601-2618.
- Dieterich, J.H. and K.B. Richards-Dinger (2010). Earthquake recurrence in simulated fault systems, *Pure Appl. Geophys.* 167, 1087-1104, doi: 10.1007/s00024-010-0094-0.
- Ellsworth, W.L., M.V. Matthews, R.M. Nadeau, S.P. Nishenko, P.A. Reasenber and R.W. Simpson (1999). A physically based earthquake recurrence model for estimation of long-term earthquake probabilities, *U.S. Geol. Surv. Open-File Rept.*, 99-522.
- Field, E.H. (2015). Computing elastic-rebound-motivated earthquake probabilities in unsegmented fault models: a new methodology supported by physics-based simulators, *Bull. Seismol. Soc. Am.*, 105, 544-559, Doi:10.1785/01201140094.
- Ganas, A., P. Elias, G. Bozionelos, G. Papathanassiou, A. Avallone, A. Papastergios, S. Valkaniotis, I. Parcharidis and P. Briole (2016). Coseismic deformation, field observations and seismic fault of the 17 November 2015 M = 6.5, Lefkada Island, Greece earthquake. *Tectonophysics*, 687, 210-222.

- Harris, R.A. (1998). Introduction to special section: stress triggers, stress shadows, and implications for seismic hazard, *J. Geophys. Res.*, 103, 24-24358.
- Harris, R.A. and R.W. Simpson (1998). Suppression of large earthquakes by stress shadows: a comparison of Coulomb and rate-and-state failure, *J. Geophys. Res.*, 103, 24-24451.
- Hatzfeld, D., I. Kassaras, D. Panagiotopoulos, D. Amorese, K. Makropoulos, G. Karakaisis, and O. Coutant (1995). Microseismicity and strain pattern in northwest Greece, *Tectonics*, 14, 773-785.
- Jenkins, D.A.L. (1972). Structural development of western Greece, *Am. Assoc. Pet. Geol. Bull.*, 56, 128-149.
- Jenny, S., S. Goes, D. Giardini, and H.-G. Kahle (2004). Earthquake recurrence parameters from seismic and geodetic strain rates in the eastern Mediterranean, *Geophys. J. Int.*, 157, 1331-1347.
- Kahle, H.G., M.V. Müller, A. Geiger, G. Danuser, S. Mueller, G. Veis, H. Billiris, and D. Paradissis (1995). The strain field in northwestern Greece and the Ionian Islands: results inferred from GPS measurements, *Tectonophysics*, 249, 1-2, 41-52.
- Karakostas, V., E. Papadimitriou and C. Papazachos (2004). Properties of the 2003 Lefkada, Ionian islands, Greece, Earthquake seismic sequence and seismicity triggering, *Bull. Seismol. Soc. Am.*, 94, 5, 1976-1981.
- Karakostas, V., E. Papadimitriou, M. Mesimeri, Ch. Gkarlaouni, and P. Paradisopoulou (2015). The 2014 Kefalonia doublet (Mw6.1 and Mw6.0) central Ionian Islands, Greece: seismotectonic implications along the Kefalonia transform fault zone, *Acta Geophys.*, 63, 1-16, doi: 10.2478/s11600-014-0227-4.
- Karakostas, V., E. Papadimitriou, P. Patias and Ch. Georgiadis (2019). Coastal deformation in Lefkada Island associated with strong earthquake occurrence, *Boll. Geofis. Teor. Appl.*, 60, 1-16, doi:10.4430/bgta0267.
- Kiratzis, A. and C. Langston (1991). Moment tensor inversion of the 1983 January 17 Kefallinia event of Ionian islands (Greece), *Geophys. J. Int.*, 105, 529-538.
- Kostoglou, A., V. Karakostas, P. Bountzias, and E. Papadimitriou (2020). The February-March 2019 Seismic Swarm Offshore North Lefkada Island, Greece: Microseismicity Analysis and Geodynamic Implications, *Appl. Sci.*, 10, 4491, doi:10.3390/app10134491.
- Kourouklas, C., R. Console, E. Papadimitriou, M. Murru and V. Karakostas (2021a). Modelling the large earthquakes recurrence times along the North Aegean Trough Fault Zone (Greece) with a physics-based simulator, *Geophys. J. Int.*, 225, 2135-2156, doi:10.1093/gji/ggab085.
- Kourouklas, C., R. Console, E. Papadimitriou, M., Murru and V. Karakostas (2021b). Strong earthquakes recurrence times of the Southern Thessaly, Greece, Fault Zone: Insights from a physics-based simulator application, *Front. Earth Sci.*, 9, 596854, doi:10.3389/feart.2021.596854.
- LePichon X and J. Angelier (1979). The Hellenic Arc and Trench system: a key to the neotectonic evolution of the eastern Mediterranean area, *Tectonophysics*, 60, 1-2, 1-42.
- Louvari, E., A.A. Kiratzis, and B.C. Papazachos (1999). The Cephalonia transform Fault and its extension to western Lefkada Island (Greece), *Tectonophysics*, 308, 223-236.
- Mangira, O., R. Console, E. Papadimitriou, M. Murru and V. Karakosta (2020). The short-term seismicity of the Central Ionian Islands (Greece) studied by means of a clustering model, *Geophys. J. Int.*, 220, 856-875.
- Mann, H.B. and D.R. Whitney (1947). On a test of whether one of two random variables is stochastically larger than the other, *Ann. Math. Stat.*, 18, 50-60.
- Margaris, B.N., and P.M. Hatzidimitriou (2002). Source spectral scaling and stress release estimates using strong-motion records in Greece, *Bull. Seismol. Soc. Am.*, 92, 1040-1059.
- Matthews, V.M., W.L. Ellsworth, and P.A. Reasenberg (2002). A Brownian model for recurrent earthquakes, *Bull. Seismol. Soc. Am.*, 92, 2233-2250.
- McKenzie, D. (1972). Active tectonics of the Mediterranean region, *Geophys. J. Roy. Astron. Soc.*, 30, 109-185.
- McKenzie, D. (1978). Active tectonics of the Alpine-Himalayan belt: the Aegean Sea and surrounding regions, *Geophys. J. Roy. Astron. Soc.*, 55, 217-254.
- Papadimitriou, E.E. (1993). Focal mechanisms along the convex side of the Hellenic Arc, *Boll. Geofis. Teor. Appl.*, 140, 401-426.
- Papadimitriou, E.E. (2002). Mode of strong earthquake occurrence in central Ionian Islands (Greece). Possible triggering due to Coulomb stress changes generated by the occurrence of previous strong shocks, *Bull. Seismol. Soc. Am.*, 92, 3293-3308.
- Papadimitriou, E., V. Karakostas, M. Mesimeri, G. Chouliaras and Ch. Kourouklas (2017). The Mw6.5 17 November 2015 Lefkada (Greece) earthquake: structural interpretation by means of the aftershock analysis, *Pure Appl. Geophys.*, 174, 3869-3888.

- Papazachos, B.C. and P. E. Comninakis (1971). Geophysical and tectonic features of the Aegean arc, *J. Geophys. Res.*, 76, 8517-8533.
- Papazachos, B.C., E.E. Papadimitriou, A.A. Kiratzi, C.B. Papazachos and E.K. Louvari (1998). Fault plane solutions in the Aegean Sea and the surrounding area and their tectonic implications, *Boll. Geofis. Teor. Appl.*, 39, 199-218.
- Papazachos, B.C. and C. C. Papazachou (2003). *The earthquakes of Greece*. Ziti Publication Co., Thessaloniki, Greece, 304.
- Papazachos, B.C., P.E. Comninakis, E.M., Scordilis, G.F., Karakaisis and C.B. Papazachos (2010). A catalogue of earthquakes in the Mediterranean and surrounding area for the period 1901-2010, *Publ. Geophys. Laboratory, University of Thessaloniki, Greece*.
- Parsons, T., E.L. Geist, R. Console and R. Carluccio (2018). Characteristic earthquake magnitude frequency distribution on faults calculated from consensus data in California, *J. Geophys. Res.*, 123, doi:10.1029/2018JB016539.
- Pasari, S., H. Verma, Y. Sharma, and N. Choudhary (2023). Spatial distribution of seismic cycle progression in northeast India and Bangladesh regions inferred from natural time analysis, *Acta Geophys.*, 71, 89-100.
- Pollitz, F.F. (2011). Epistemic uncertainty in California-wide synthetic seismicity simulations, *Bull. Seismol. Soc. Am.*, 101, 2481-2498.
- Pollitz, F.F. (2012). ViscoSim earthquake simulator, *Seismol. Res. Lett.*, 83, 979-982.
- Pollitz, F.F. and D. Schwartz (2008). Probabilistic seismic hazard in the San Francisco Bay area based on a simplified viscoelastic-cycle model of fault interactions, *J. Geophys. Res.* 113, B05409, doi: 10.1029/2007JB005227.
- Reid, H.F. (1911). The elastic-rebound theory of earthquakes, University of California Publications, *Bulletin of Department of Geological Science*, 6, 413-444.
- Richards-Dinger, K. and J.H. Dieterich (2012). RSQSim earthquake simulator, *Seismol. Res. Lett.*, 83, 983-990, doi: 10.1785/0220120105.
- Robinson, R. and R. Benites (1996). Synthetic seismicity models for the Wellington Region, New Zealand: implications for the temporal distribution of large events, *J. Geophys. Res.*, 101 (27), 833-844, doi:10.1029/96jb02533.
- Rundle, J.B. (1988). A physical model for earthquakes. 2. Application to southern California, *J. Geophys. Res.*, 93, 6255-6274, doi:10.1029/jb093ib06p06255.
- Rundle, J.B., P.B. Rundle, A. Donnellan, D. Turcotte, R. Scherbakov, P. Li, B.D. Malamud, L.B. Grant, G.C. Fox, D. McLeod, et al. (2005). A simulation-based approach to forecasting the next great San Francisco earthquake, *Proc. Natl. Acad. Sci. Unit. States Am.*, 102, 15,363-15,367.
- Schwartz, D.P. and K.J. Coppersmith (1984). Fault behavior and characteristic earthquakes: examples from Wasatch and San Andreas fault zones, *J. Geophys. Res.*, 89, 5681-5698.
- Scordilis, E., G.F. Karakaisis, V. Karakostas, D.G. Panagiotopoulos, P.E. Comninakis, and B.C. Papazachos (1985). Evidence for Transform Faulting in the Ionian Sea: The Cephalonia Island Earthquake Sequence of 1983, *Pure Appl. Geophys.*, 123, 388-397.
- Schultz, K.W., M. Sachs, M.R. Yoder, J.B. Rundle, D.L. Turcotte, E.M. Helen and A. Donnellan (2015). Virtual quake: Statistics, co-seismic deformations and gravity changes for driven earthquake fault systems, in M. Hashimoto (Editor), *International Symposium on Geodesy for Earthquake and Natural Hazards (GENAH)*, International Association of Geodesy Symposia, 145, Springer, Cham, Switzerland.
- Schultz, K.W., M.R. Yoder, J.M. Wilson, E.M. Heien, M.K. Scahs, J.B. Rundle and D.L. Turcotte (2017). Parametrizing physics-based earthquake simulations, *Pure Appl. Geophys.*, 174, 2269-2278.
- Stephens, M.A. (1974). EDF statistics for goodness of fit and some comparisons, *J. Am. Stat. Assoc.*, 64 (374), 730-737, doi:10.2307/2286009.
- Stiros, S.C., P.A. Pirazzoli, J. Laborel, and F. Laborel-Deguen (1994). The 1953 Earthquake in Cephalonia (Western Hellenic Arc): Coastal uplift and halotectonic faulting, *Geophys. J. Int.*, 117, 834-849. Doi: 10.1111/j. 1365-246X.1994.tb02474.x.
- Sykes, L.R. and W. Menke (2006). Repeat times of large earthquakes: implications for earthquake mechanics and long-term prediction, *Bull. Seismol. Soc. Am.*, 96, 1569-1596, doi:10.1785/0120050083.
- Svigkas, N., S., Atzori, A., Kiratzi, C., Tolomei, A., Antonioli, I., Papoutsis, S., Salvi and C., Kontoes (2019). On the Segmentation of the Cephalonia-Lefkada Transform Fault Zone (Greece) from an InSAR Multi-Mode Dataset of the Lefkada 2015 Sequence, *Remote Sens.*, 11, 1848, doi:10.3390/rs11161848.
- Toda, S., R.S. Stein, P.A. Reasenberg and J.H. Dieterich (1998). Stress transfer by the 1995 $M_w = 6.9$ Kobe, Japan, shock: effect on aftershocks and future earthquake probabilities, *J. Geophys. Res.*, 103, B10, 24, 543-24,565.
- Toda, S. and R.S. Stein (2003). Toggling of seismicity by the 1997 Kagoshima earthquake couplet: a demonstration of time-dependent stress transfer, *J. Geophys. Res.*, 108, B12, 2567, doi:10.1019/2003JB002527.

Simulated Recurrence Times along KTFZ

- Tullis, T.E. (2012). Preface to the focused issue on earthquake simulators, *Seismol Res. Lett.*, 83, 957-958, doi:10.1785/0220120122.
- Underhill, J.R. (1989). Late Cenozoic deformation of the Hellenide foreland, western Greece, *Geol. Soc. Am. Bull.*, 101, 613-634.
- Ward, S.N. (2000). San Francisco Bay area earthquake simulators: a step toward a standard physical earthquake model, *Bull. Seismol. Soc. Am.*, 90, 370-386.
- Wessel, P., W.H.F. Smith, R. Scharroo, J.Luis, and F. Wobbe (2013). Generic mapping tools: Improved version released, *EOS, Tran. Am. Geophys. Union*, 2013, 94, 409-410.
- Wilcoxon, F. (1945). Individual comparisons by ranking methods, *Biometrics*, 1, 80-83.

***CORRESPONDING AUTHOR: Christos KOUROUKLAS,**

Geophysics Department, School of Geology, Aristotle University of Thessaloniki, GR54124 Thessaloniki, Greece
e-mail: ckouroukl@geo.auth.gr.